NAGW-1736

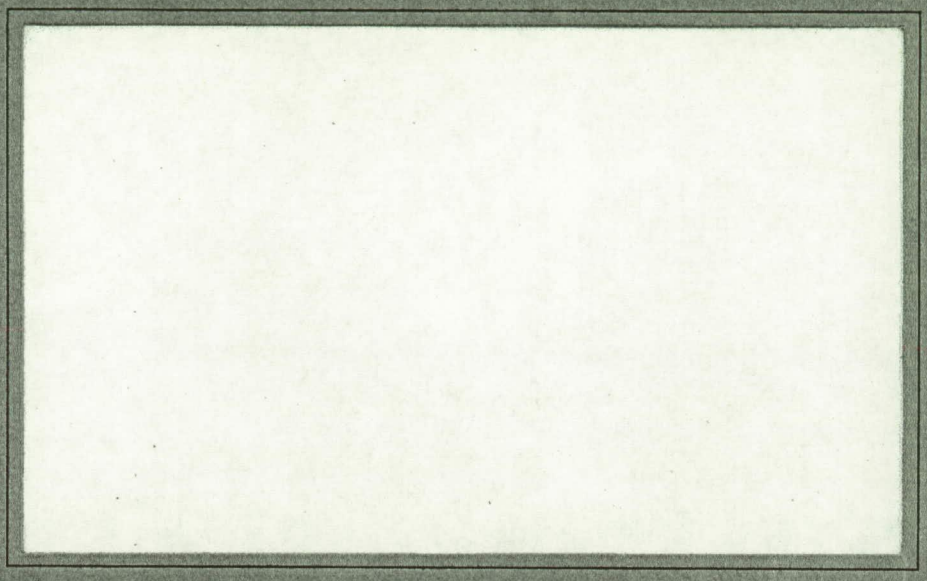

INSTITUT FÜR RAUMFAHRTSYSTEME
UNIVERSITÄT STUTTGART

PFAFFENWALDRING 31

7000 STUTTGART 80 (VAIHINGEN)

High Power Arcjet

T. M. Gölz, M. Auweter-Kurtz,
H. L. Kurtz, and H. O. Schrade

Institut für Raumfahrtsysteme
University of Stuttgart
IRS 91–P3

Third Progress Report
NASA Grant No. NAGW–1736
for NASA Lewis Research Center, Cleveland, OH

February 1991

Contents

Abstract

This third progress report covers the activities on the high power arcjet project from August 1990 to January 1991.

In this period the HIPARC thruster was ignited for the first time, and in the following tests power levels up to 140 kW with a mass flow rate of 300 mg/s hydrogen were reached. Specific impulse values of more than 1300 s were shown to be possible. Tests have been performed with the baseline thruster version only, which has a 6 mm throat diameter and a conical nozzle with a 20° half angle.

Measurement data summing up all tests carried out until now is included. All measuring methods are described, including a check on possible error sources.

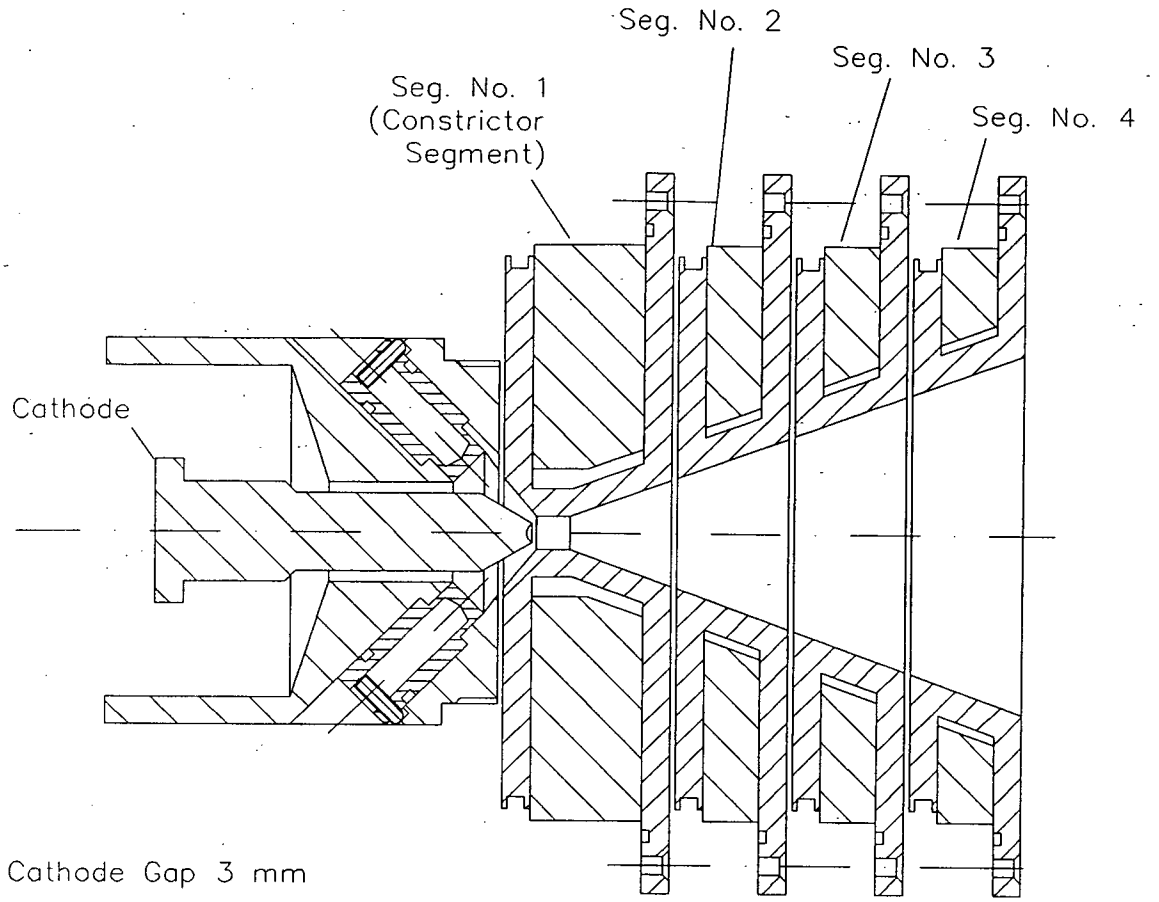

Figure 1: Cut away drawing of the HIPARC nozzle section as tested in the runs reported

1 Measuring Methods

1.1 Current and Voltage Measurements

The electrical magnitudes current and voltage are measured as shown in the circuit diagram below (see Fig. 2).

Three segment currents are measured by means of shunt resistors R_1, which are mounted beneath the thruster inside the vacuum tank. These shunts provide a voltage drop of 60 mV at 1000 A, which is full scale. Measuring cables lead to insulation amplifiers outside the tank. The total current is measured by an additional shunt resistor R_2 mounted outside the tank. This shunt is designed for a maximum current of 2000 A, providing a 150 mV voltage drop at full scale. The constrictor segment current is calculated by subtracting the sum of the three other segment currents from the total current.

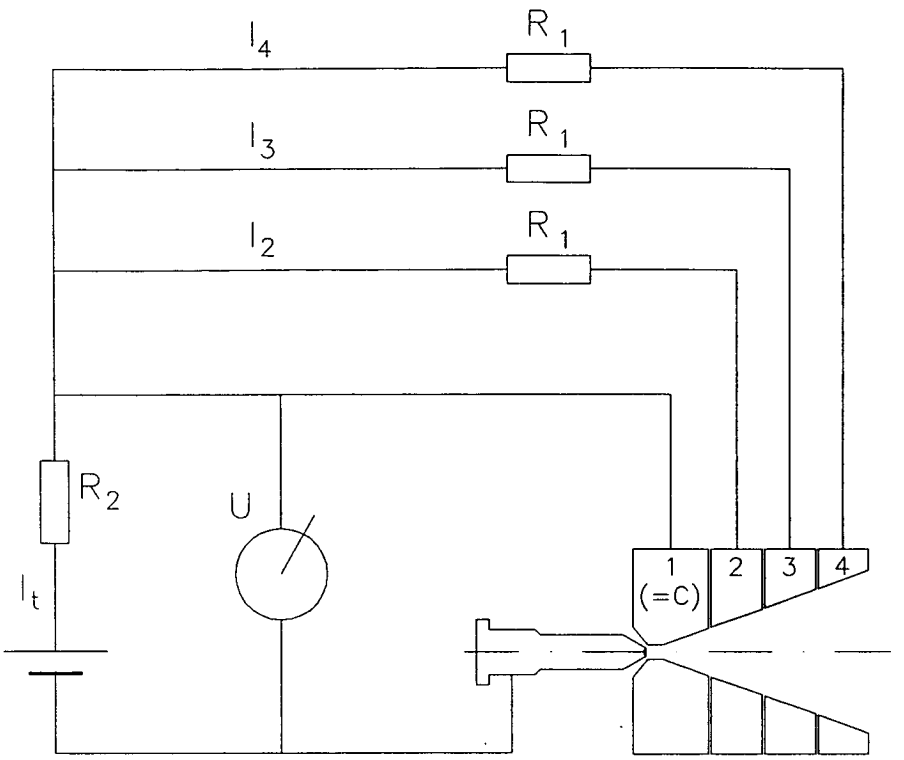

Figure 2: Circuit diagram of the HIPARC experiment

The shunt accuracy is ± 0.5 %, which results in tolerances in the segment currents of 5 A, and 10 A in the total current, respectively.

The arc voltage is measured directly with an isolation amplifier with a full scale voltage of 200 V. The relative accuracy is ± 0.5 %, which is an absolute tolerance of ± 1 V.

1.2 Pressure Measurements

The arc chamber pressure is measured by a HBM absolute pressure cell of the strain gauge type with a full scale range of 5 bar. The relative accuracy is given as $< \pm$ 0.3 %, which is equivalent to an absolute accuracy of $< \pm 15$ mbar.

The ambient pressure is measured by a Convectron pressure gauge, which is calibrated for nitrogen. The readout is corrected for hydrogen by the experimant software. The gauge reaches an accuracy of ±5 %, referred to the measured value.

Typical background pressure with a mass flow rate of 300 mg/s is 0.15 mbar.

1.3 Thrust Measurement

The thrust is measured by means of the thrust balance described in the first progress report [1].

The thrust measurement has caused serious problems in the period reported. The tank lid was considerably deformed due to the pressure difference when the tank was evacuated. The deformation of the center of the lid was 2.34 mm, the bracket where the balance was mounted was bended 5 mm upwards its tip. This was the reason for the current supply rods touching the mercury filled tubes on their front side. The problem could be solved by inserting a flexible part to the current feed, which allows a decoupling of the balance from the center of lid deformations. The bracket deformation was compensated by adjusting the bracket so that it would be horizontal under vacuum conditions.

In order to get a higher accuracy a new force tranducer was built in. This transducer's full scale range is a mass equivalent of 2 kg, compared to the 5 kg range of the old one. This change of gauges effects the accuracy of thrust measurement in two ways: First the theoretical error of the load cell was cut down to 40 % of what it had been before, simply because of the smaller full scale range. Second the new cell provides a higher output voltage, so that the resolution could be increased from $6.2 \cdot 10^{-3}$ N to $6.5 \cdot 10^{-4}$ N.

The theoretical error limits depending on electrical magnitudes only are $\pm$ 0,01 N now.

Other errors originate from frictional influences, and from vibrations of the high pressure cooling water supply. These effects cause additional errors, so that the total error results in < 0.04 N. Fig. 3 and Fig. 4 show a plot of calibration measurement data before test run No. 12. The horizontal lines show the error limit of ± 0.04 N.

In addition there were drifting effects on the thrust measurement, which could not yet be fully explained. Thermal drifting was expected, but the observed phenomena showed a drift in calibration runs without the thruster operating, but with the cooling water running. It was showed that this effect originates from low pressure water cooling of the force transducer. Typical times for this effect are 50 min, where steady state temperature conditions in the balance can be assumed. This behaviour did not effect measurement accuracy in the tests performed because of the short test cycle length. Further investigations on these effects are scheduled.

1.4 Mass Flow Rate Measurement

The mass flow rate is measured by mass flow controllers of the thermal type, which are selected individually according to the desired flow rate. All controllers are

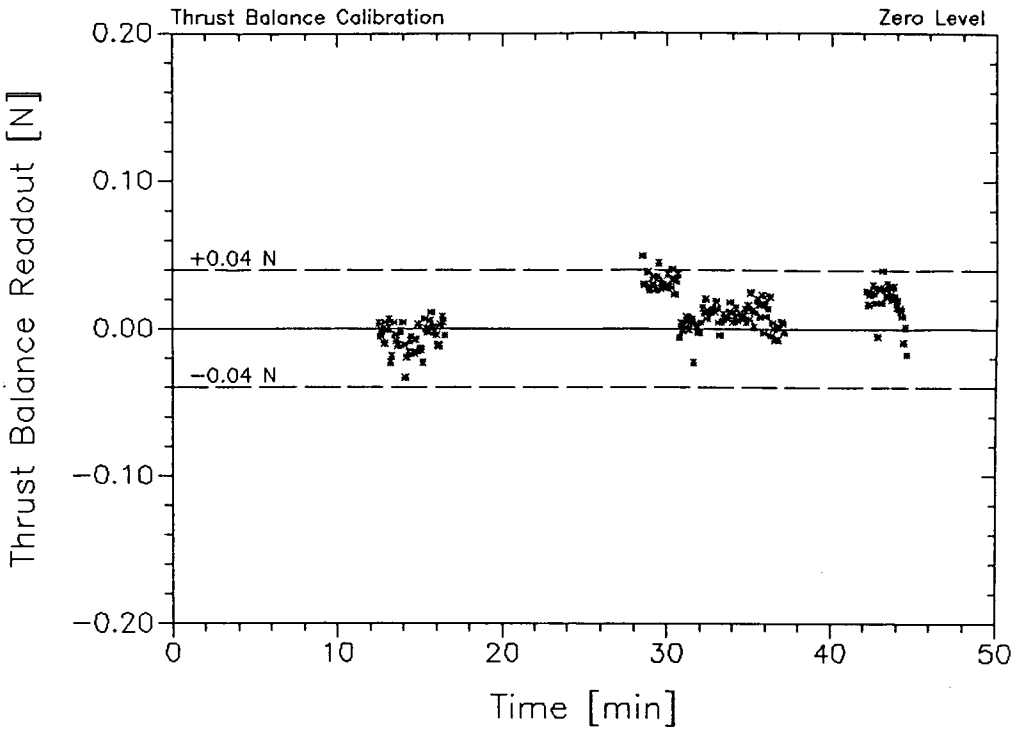

Figure 3: Thrust balance calibration: Zero level

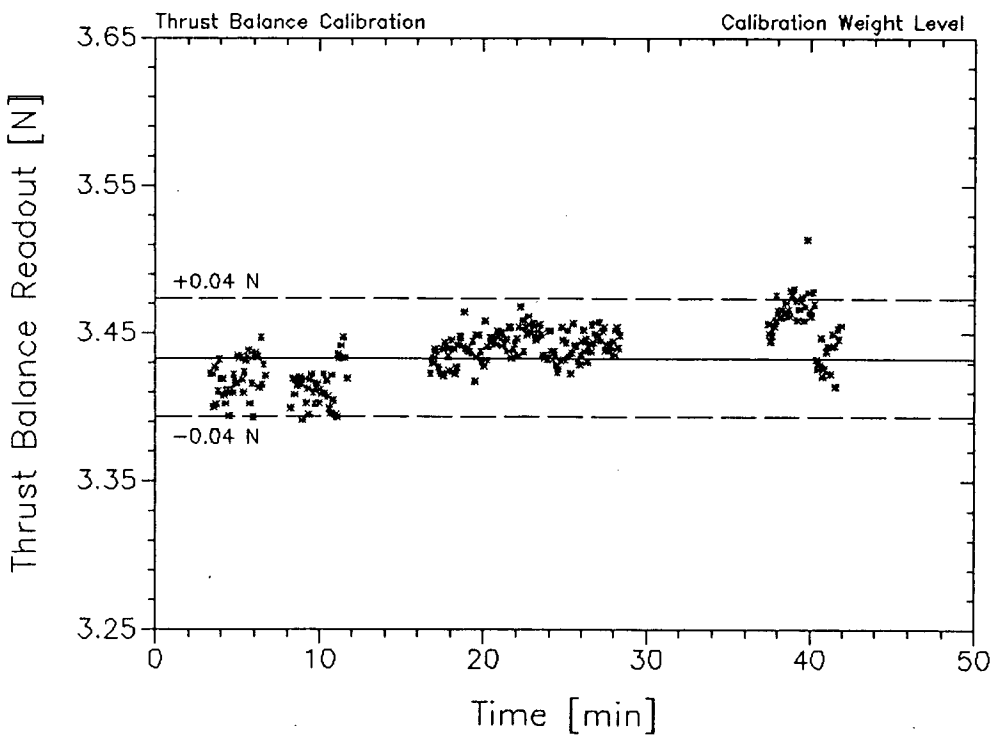

Figure 4: Thrust balance calibration: Calibration weight level

calibrated for hydrogen. There are three different controllers available which are calibrated for hydrogen. Two of them are manufactured by Tylan, providing a full scale range of 30 slpm and 200 slpm, respectively. The third one provides a full scale range of 400 slpm; it is the manufactured by Teledyne Hastings-Raydist. The accuracy is given as ± 1 % of full scale, which means an absolute tolerance value of ± 2 slpm hydrogen in all the tests presented here. This is equivalent to a mass flow tolerance of ± 3 mg/s.

1.5 Heat Flux Measurement

Neglecting the radiation of heat from the thruster body to the vacuum tank and considering only steady state conditions the heat flux into the segments can be determined by measuring the heat flux into the cooling water, which is calculated from temperature difference and water flow rate measurements.

Temperatures are taken from PT 100 platinum resistance thermometers. The flow rates through each segment are determined by measuring the total flow rate, and multiplying it with correlation factors evaluated in calibration experiments before. The accuracy of these PT 100 thermometers is ± 0.1 K, the water flow can be measured with an accuracy of ± 0.01 kg/s. This results in a heat flux accuracy between ±0.15 kW and ±0.36 kW, increasing with temperature difference.

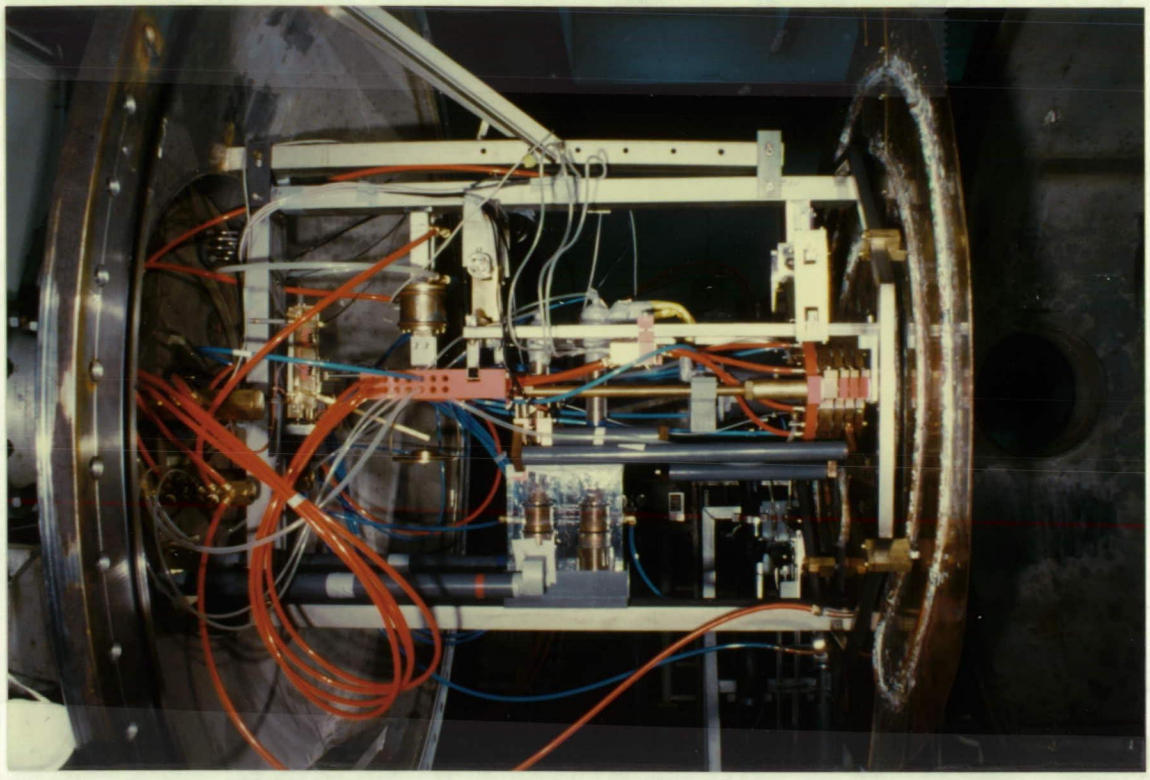

Figure 5: HIPARC thruster mounted on the thrust balance

2 Experimental Results

The baseline thruster was run with a 6 mm nozzle throat diameter and hydrogen as propellant. A range of 10–40 kW at 100 mg/s mass flow rate, 15–90 kW at 200 mg/s, and 30–140 kW at 300 mg/s could be reached. This is equivalent to a specific input power range between 70 and 460 MWs/kg at all investigated mass flow rates.

The thruster performed very well, and the plasma plume was symmetric and stable (see Fig. 6). Only near its power limits, both upper and lower, the plume became unstable. This was the reason for engine shut down, except at the 300 mg/s mass flow rate, where cathode spitting was observed due to cathode tip overheating.

Pictures 7 and 8 show the HIPARC cathode before and after the tests. The cathode shaft diameter was 14 mm, the tip cone had a 60° full angle and a deepening of 2 mm radius. The cathode arc attachement was in the conical part of the tip only. At maximum power a melting zone could be observed in the tip deepening; spitting occured. This indicates that the cathode tip must be modified for higher power levels. Nevertheless, the cathode shape fitted to the design power level of 100 kW very well.

The following sections give a more detailed description of the measurements.

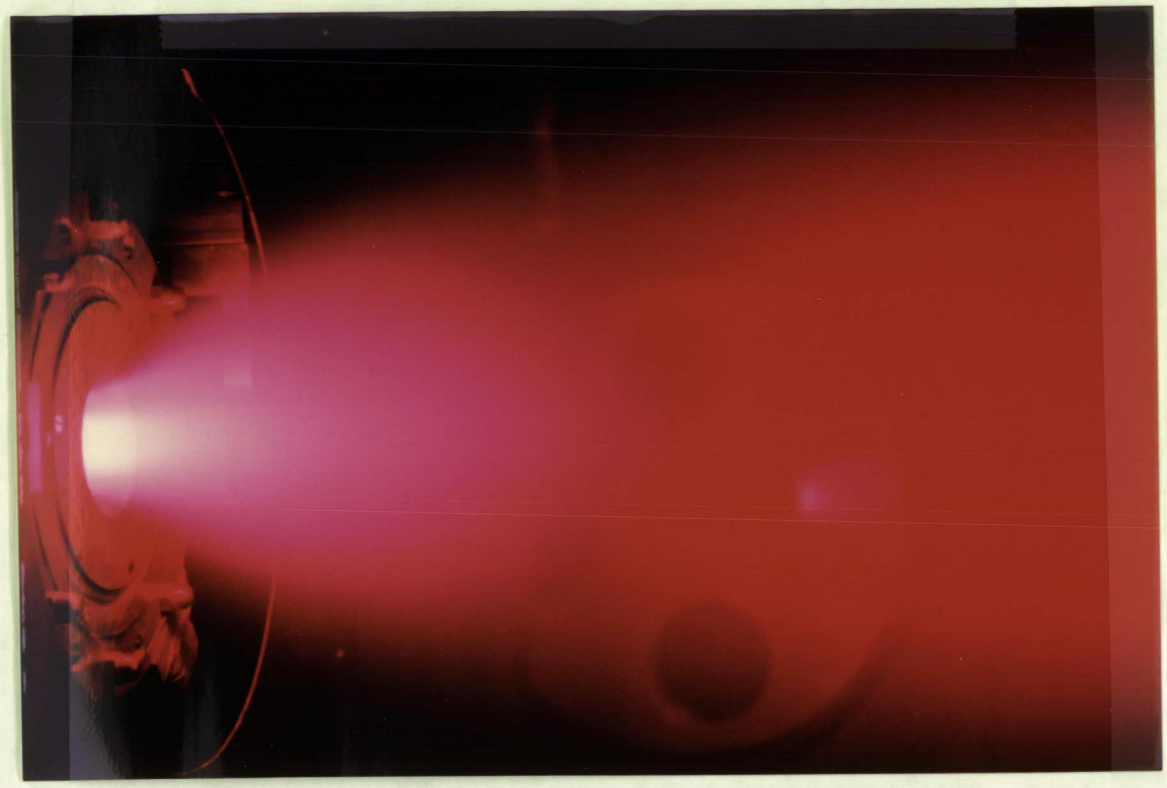

Figure 6: HIPARC running with hydrogen

Figure 7: HIPARC cathode before testing

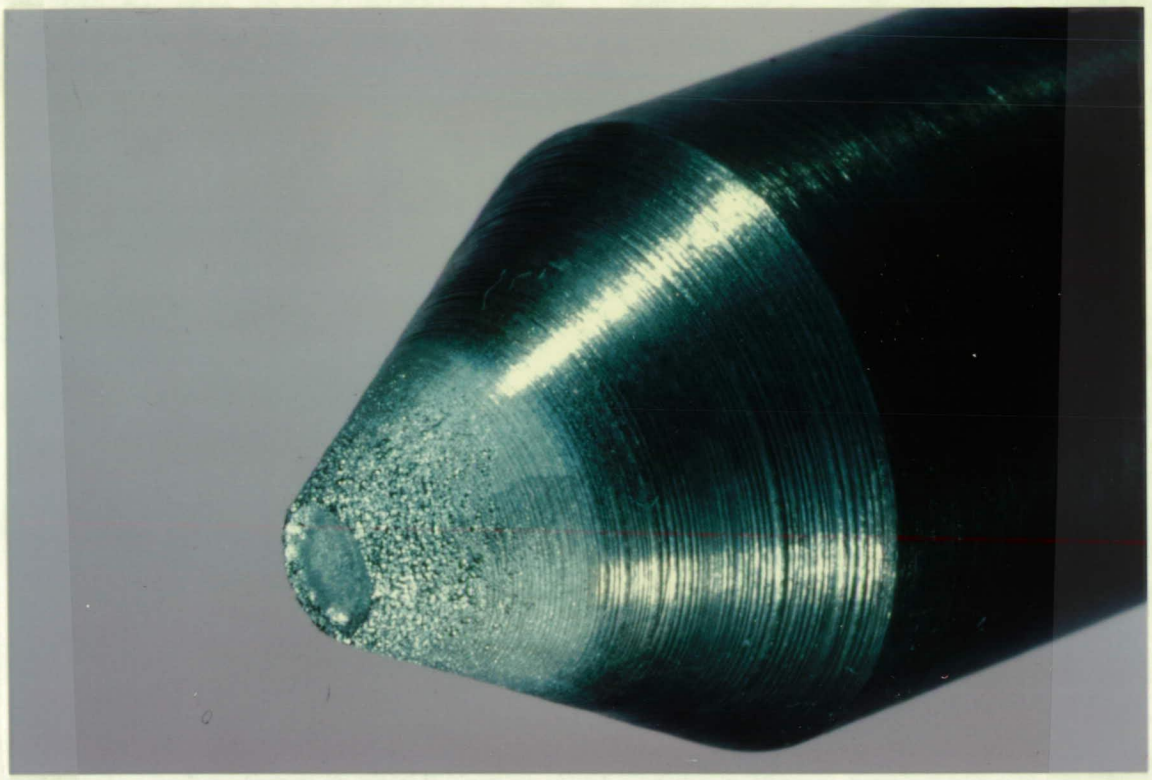

Figure 8: HIPARC cathode No. 1 after 4 test runs

2.1 Repeatability

The measurement data are repeatable quite well. Fig. 9 shows the current voltage characteristic from three different test runs. The thruster was completely dismounted after test No. 6. Main attention was directed on exact cathode centering and adjustment of the cathode gap, which was 3 mm in all tests carried out.

2.2 Current–Voltage Characteristics

A decrease in voltage with increasing current could be observed at lower power levels, as well as at higher mass flow rates. This is a typical behaviour for thermal arcjets.

A positive-slope characteristic, i.e. an increase of voltage with an increase of current, is measured at higher power levels, and at lower mass flow rates as well.

At a mass flow rate of 300 mg/s a drop of arc voltage near the upper power limit is observed. The current distribution characteristic at this mass flow rate shows a shift of current from segment No. 4 to No. 3, and from segment No. 2 to the constrictor segment, respectively. It is assumed that this is phenomenon is induced by a diminuition and destabilization of the arc surrounding cold gas mantle which

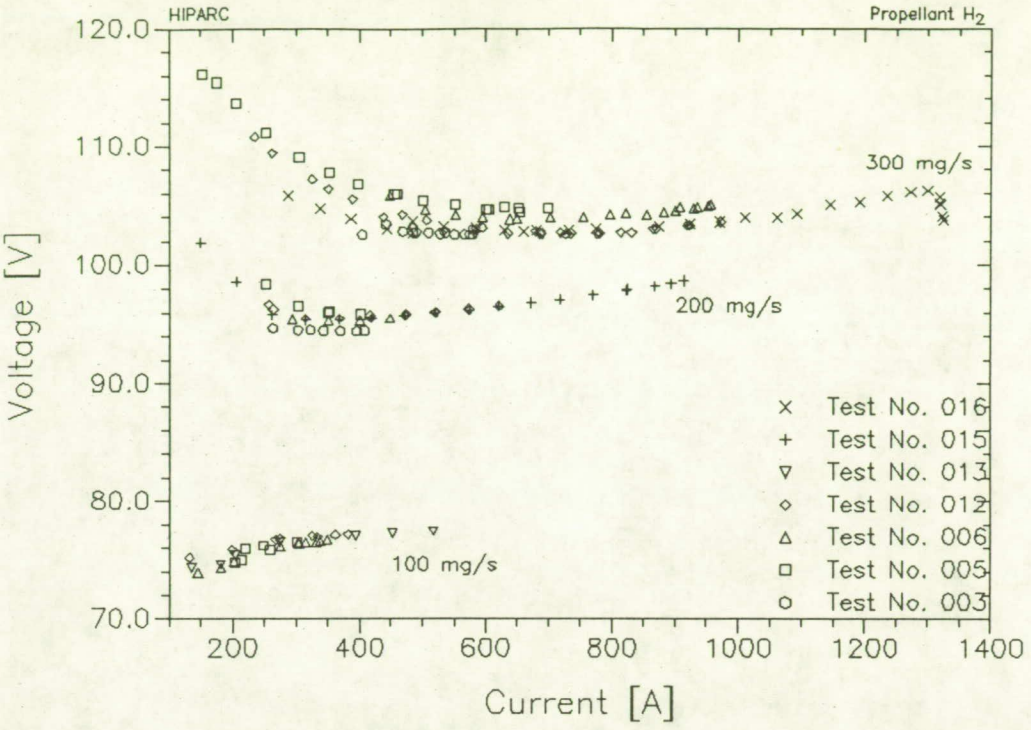

Figure 9: Current / voltage characteristics from different test runs

prevents the arc from attaching to the constrictor wall.

2.3 Current Distribution

The current distribution characteristic depends very much on the mass flow rate.

At 100 mg/s (see Fig. 11) a portion of 50–60 % of the total current is detected in segment No. 2, which is the next segment downstream of the constrictor. This indicates that the arc mainly attaches in this part of the nozzle. At lower power levels (10–15 kW, being equivalent to a specific power level of 100–150 MWs/kg) the portion of segment No. 3 was slightly higher than its values at higher power, while both upstream segments No. 1 (constrictor segment) and No. 2 were below their values at higher power.

At 300 mg/s (see Fig. 12) the characteristic is vice versa: At lower power levels the upstream segments (No. 1 and 2) collect up to 70 % of the total current. This percentage decreases to 50 % at high power. The nozzle end segment (No. 4) starts at about 15 % of the total current at low power, increasing steadily to almost 40 % at 140 kW. The current into segment No. 3 continuously stays at 10 % of the total current. At this mass flow rate the characteristic is the most evenly distributed one.

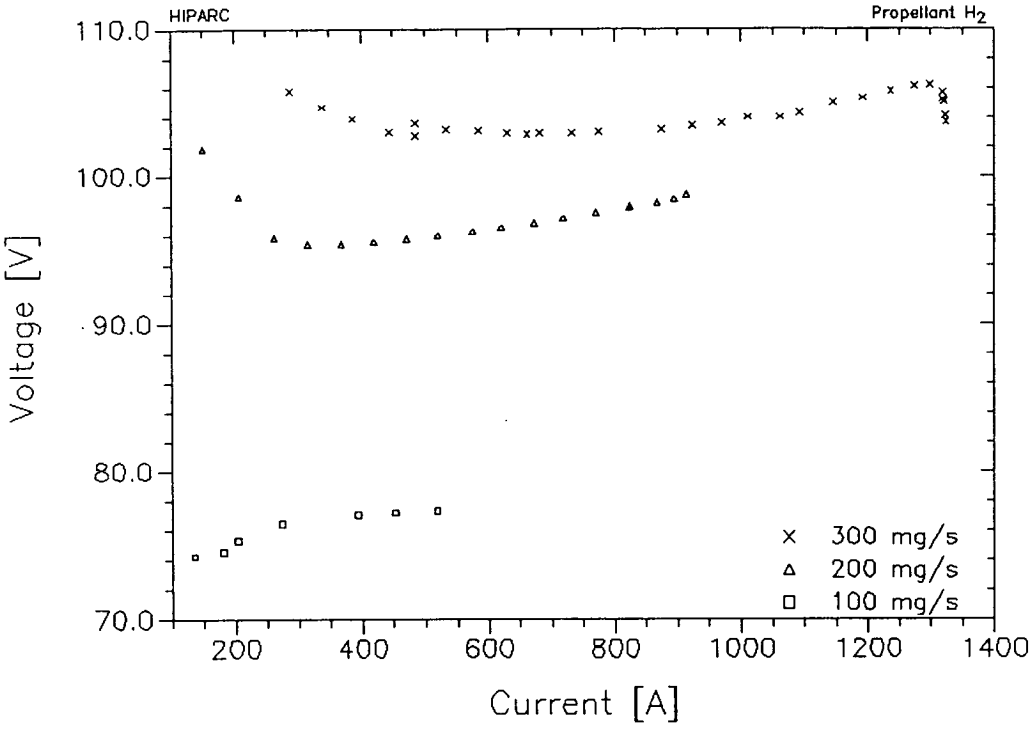

Figure 10: Current / voltage - characteristics at three different mass flow rates

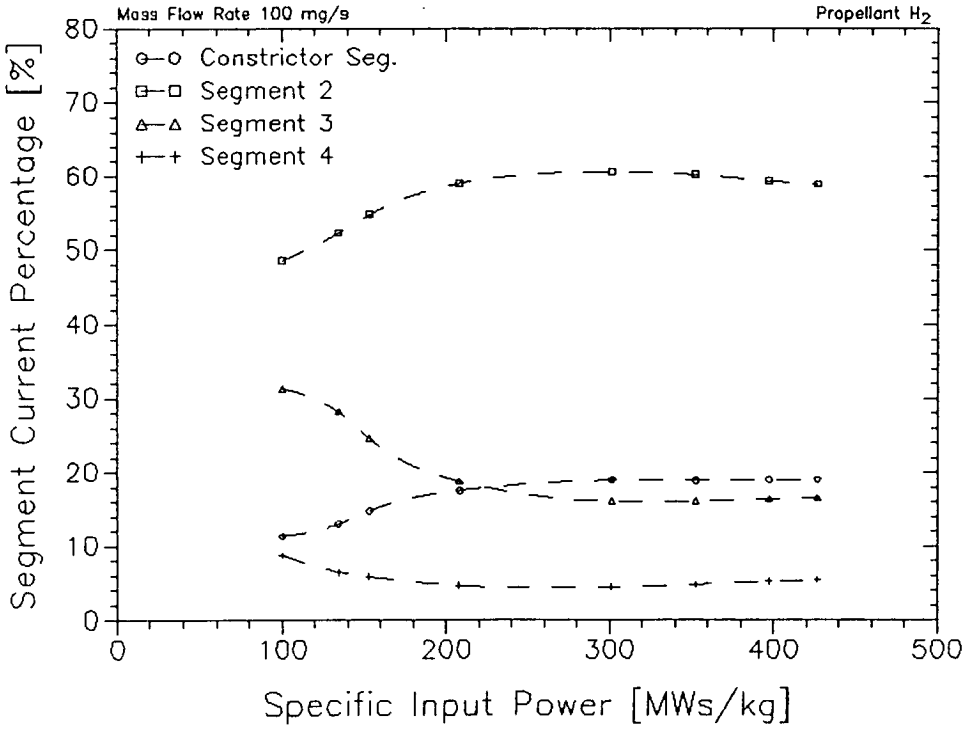

Figure 11: Current distribution in the nozzle at 100 mg/s

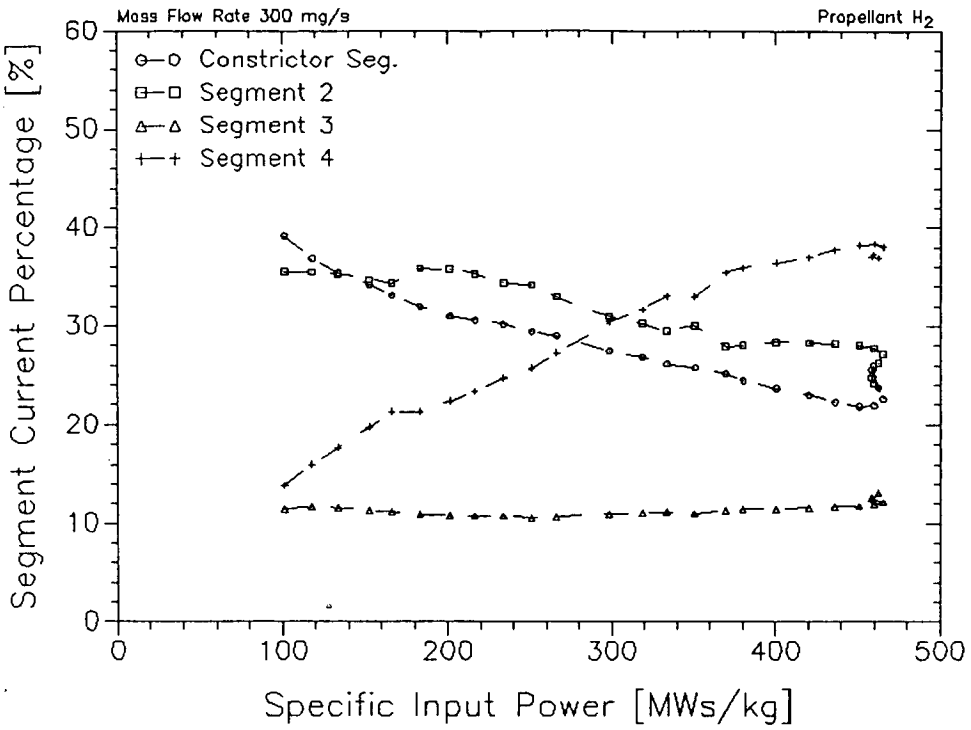

Figure 12: Current distribution in the nozzle at 300 mg/s

At a mass flow rate of 200 mg/s (see Fig. 13) most of the current could be detected in segment No. 4, which collects about 50 % of the total current at nearly all power levels, with the exception of the very low specific input power of 100 W/mg. Segments No. 1 and 2 start at low powers at 35 % and 25 % of the total current, respectively, decreasing rapidly down to 15 % and 10 %. The two upstream segments No. 3 and 4 start at 15 % and 25 %, increasing fast to values around 45–50 % (Seg. No. 4) and 25–30 % (Seg. No. 3)

This behavior could not yet be explained consistently. Like all measurement data presented here, these results are repeatable.

2.4 Thrust Characteristics

In our thrust measurement we still have to deal with thermal drifting effects of our thrust balance. This is the reason why it is not possible to provide reliable thrust data for all tests.

Nevertheless, it was possible to check thermal drifting after each test by comparing the post-test thrust values with cold gas and without gas with these values measured before the test. Using these post-test values we were able to correct at least the last few measured values.

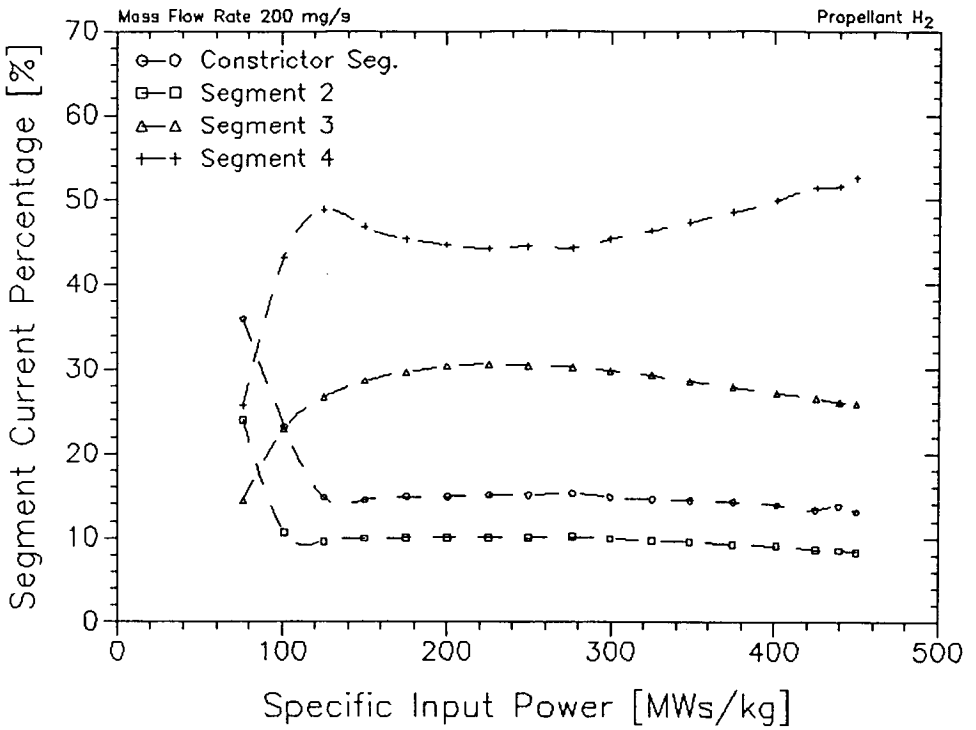

Figure 13: Current distribution in the nozzle at 200 mg/s

The best results were obtained in test runs No. 13 (Mass flow rate 100 mg/s, thermal drift -0.006 N) and No. 15 (Mass flow rate 200 mg/s, thermal drift 0.04 N).

The measured cold gas thrust values are 0.24 N at a mass flow rate of 100 mg/s, and 0.47 N at 200 mg/s. These values correspond to theoretical values of 0.27 N and 0.53 N at an assumed arc chamber temperature of 273 K under cold gas conditions. It is assumed that the nozzle end pressure equals the ambient tank pressure.

The MPD thrust portion was also calculated. An MPD thrust value of 0.12 N at 1010 A total current and of 0.29 N at 1320 A are obtained in a "worst case" calculation, where the largest segment diameter was taken as anode diameter. The radius of the deepening at the cathode tip (2 mm) was taken as cathode radius.

Figs. 14 and 15 show curves of thrust and specific impulse against electric input power. They show a positive, but decreasing slope, which indicates that an increasing portion of the total input power cannot be transformed to thrust power. Maximum specific impulse values of $1\,270 \pm 80$ s at a mass flow rate of 100 mg/s, $1\,390 \pm 40$ s at 200 mg/s, and at 300 mg/s $1\,350 \pm 25$ s at an efficiency of 18 % could be obtained. These values are corrected with the zero-thrust after switch-off.

Fig. 16 shows the thrust efficiency versus specific impulse characteristic. Thrust efficiency lies between 18 and 25 %, which is higher than it was with the TT50 thruster, which reached slightly above 15 % (See Ref. [2, 3]).

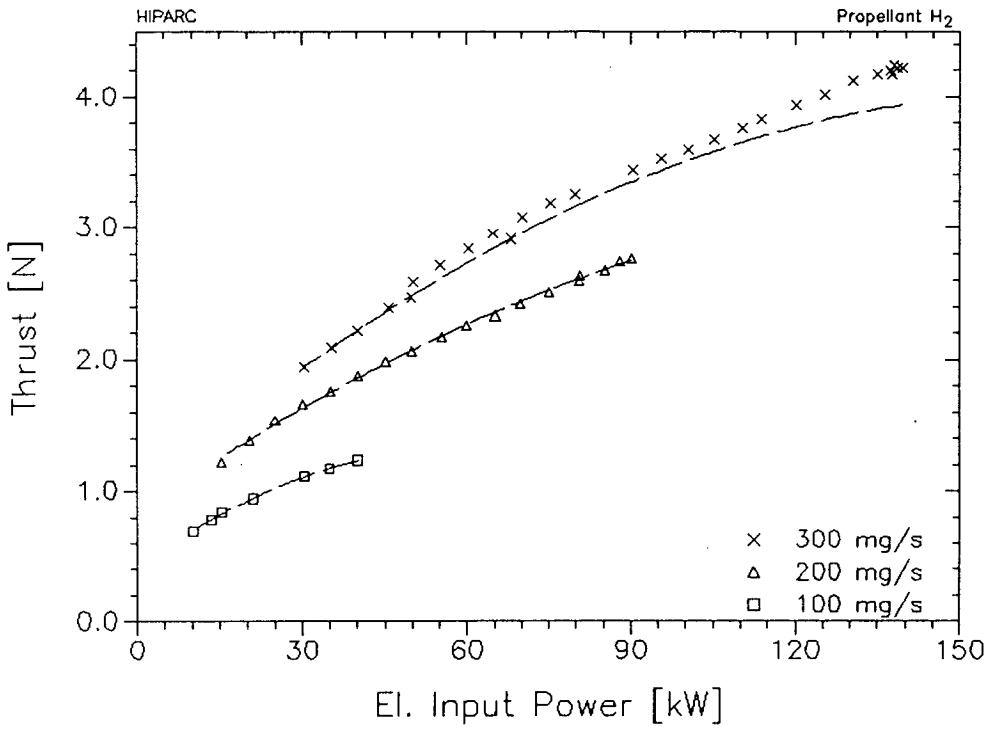

Figure 14: Thrust versus electric input power (Continuous lines represent corrected value regression lines)

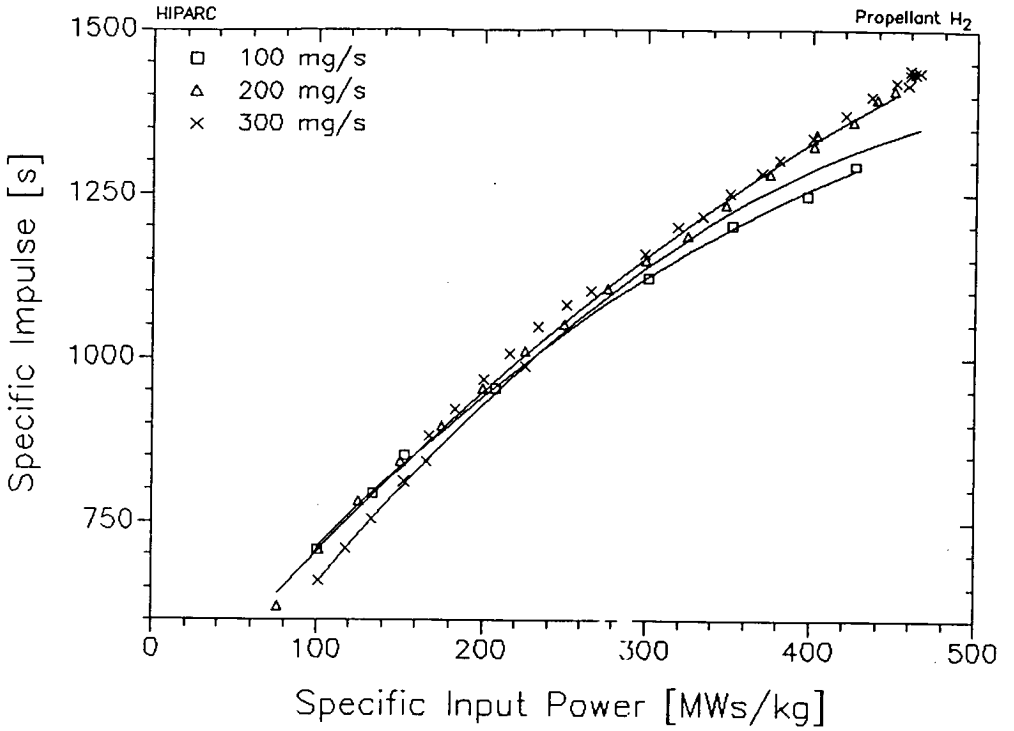

Figure 15: Specific impulse versus electric input power (Continuous lines represent corrected value regression lines)

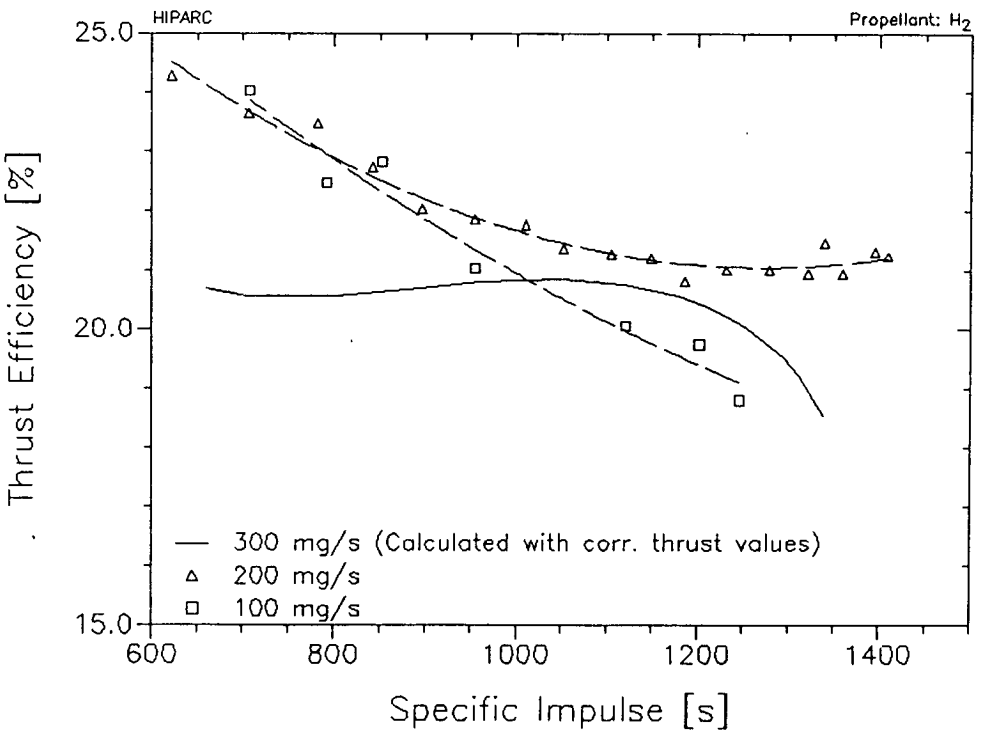

Figure 16: Thrust efficiency versus specific impulse

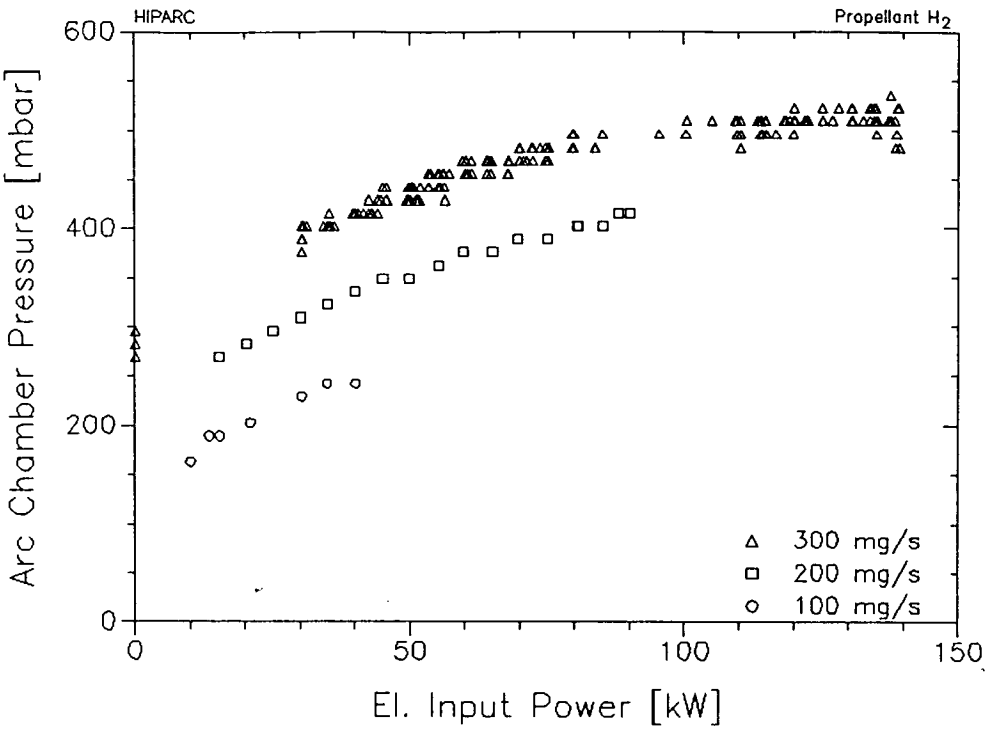

Figure 17: Arc chamber pressure versus electric input power

2.5 Arc Chamber Pressure Characteristic

The arc chamber pressure is low with the 6 mm throat diameter. The highest values reach slightly above 500 mbar, which are normally typical values for an MPD thruster (Fig. 17). The arc chamber pressure versus specific power characteristic is positive but decreasing, which is similar to the thrust against input power characteristic.

Fig. 18 shows the thrust versus arc chamber pressure characteristic.

2.6 Heat Flux and Thermal Efficiency Characteristics

The thermal efficiency was calculated as the difference of electric input power and the heat flux into the cooling water referred to the input power.

The total heat flux against input power characteristics are almost straight lines, with slopes decreasing with increasing mass flow rate (Fig. 19). This indicates a growing thermal efficiency with higher mass flows, which is shown in the thermal efficiency versus specific input power plot (Fig. 20). In this diagram the two curves of the two higher mass flow rates show a positive decreasing slope, while a negative increasing slope is observed at the 100 mg/s mass flow rate. A possible explanation

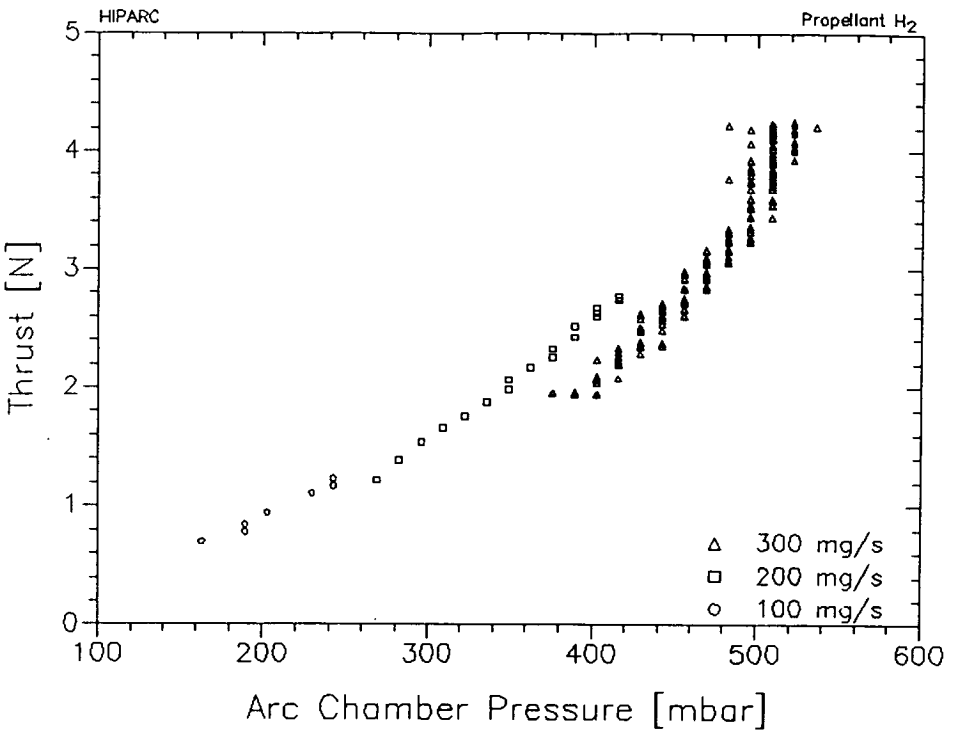

Figure 18: Thrust versus arc chamber pressure

for this could be that in the later case the cold gas mantle is effective only at lower power levels because of the lower overall pressure at lower mass flow rates. In the case of higher mass flow rates the arc is more constricted, and an increase of input power cannot be fully transported to the nozzle walls up to a certain power level.

In order to check how the current distribution measurement corresponds to the heat flux measurement, the electrical input power per segment, which is calculated as the product of arc voltage and segment current, was plotted against the segment heat flux. A good correlation between these magnitudes was expected with nearly the same heat flux to input power ratio for all segments at a constant mass flow rate.

Figs. 21, 22, and 23 show these plots for all investigated mass flow rates. In fact, the figures look different from what was expected. A comparison with the current distribution characteristics (Figs. 11–12) shows that the segments with the smallest current portion have highest slope in the heat flux versus input power plot. This indicates that the segments with low current portions get more heat than they should compared to the input power. The most likely explanation for this is that additional heat is radiated from the arc column to the wall. This effect is stronger at low mass flow rates.

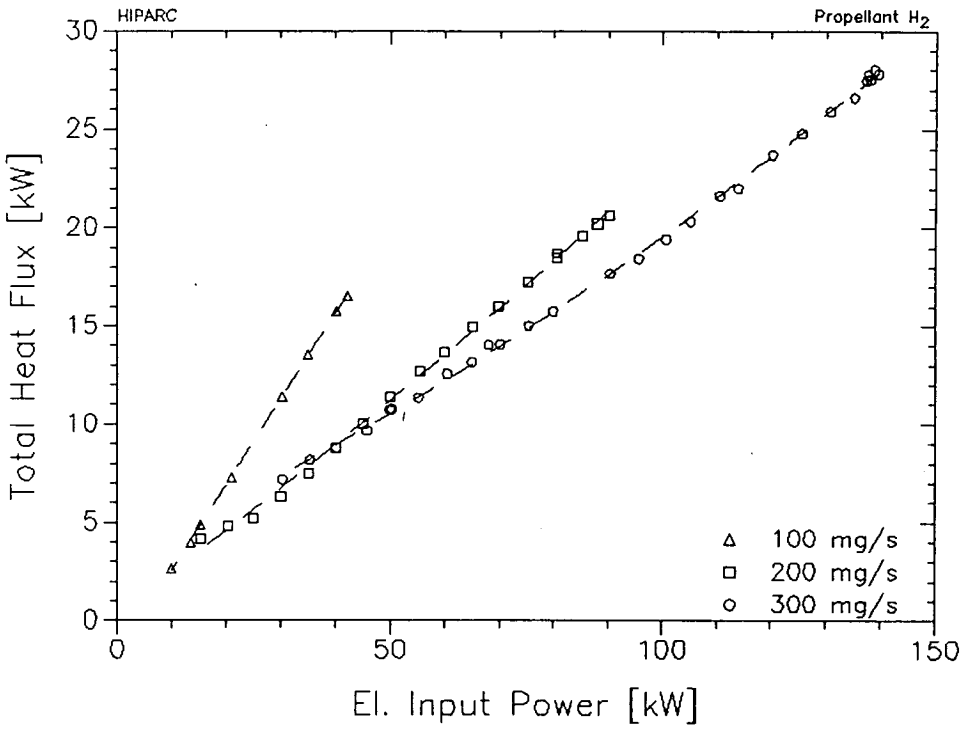

Figure 19: Cooling water losses versus electric input power, measuring points and parabolic regression lines

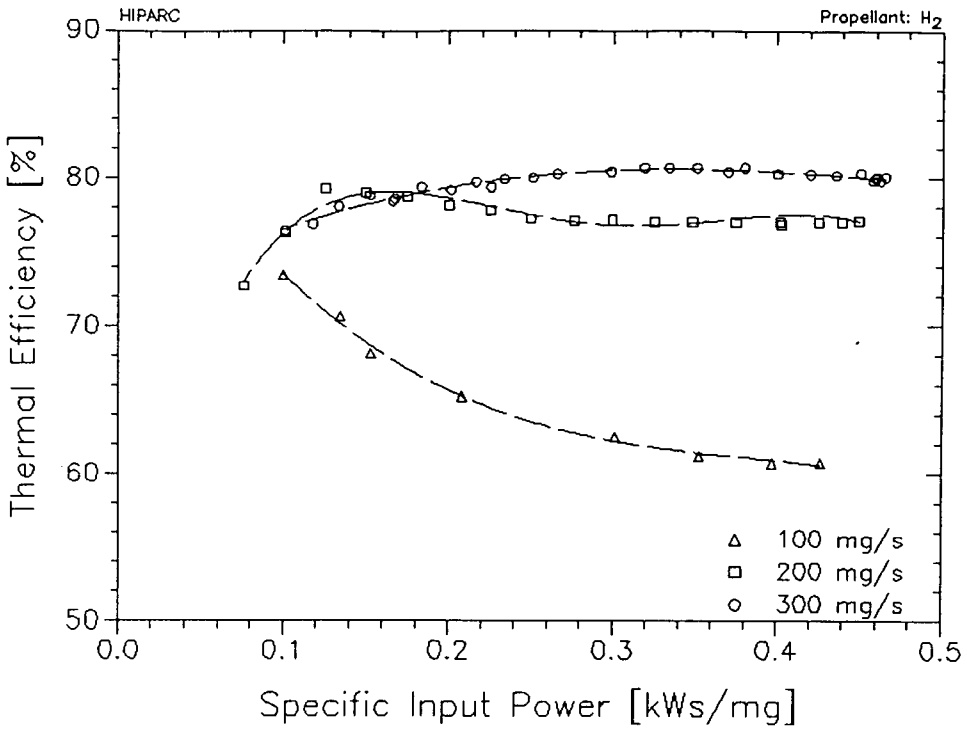

Figure 20: Thermal efficiency versus specific input power, measuring points and 2nd and 3rd order regression lines

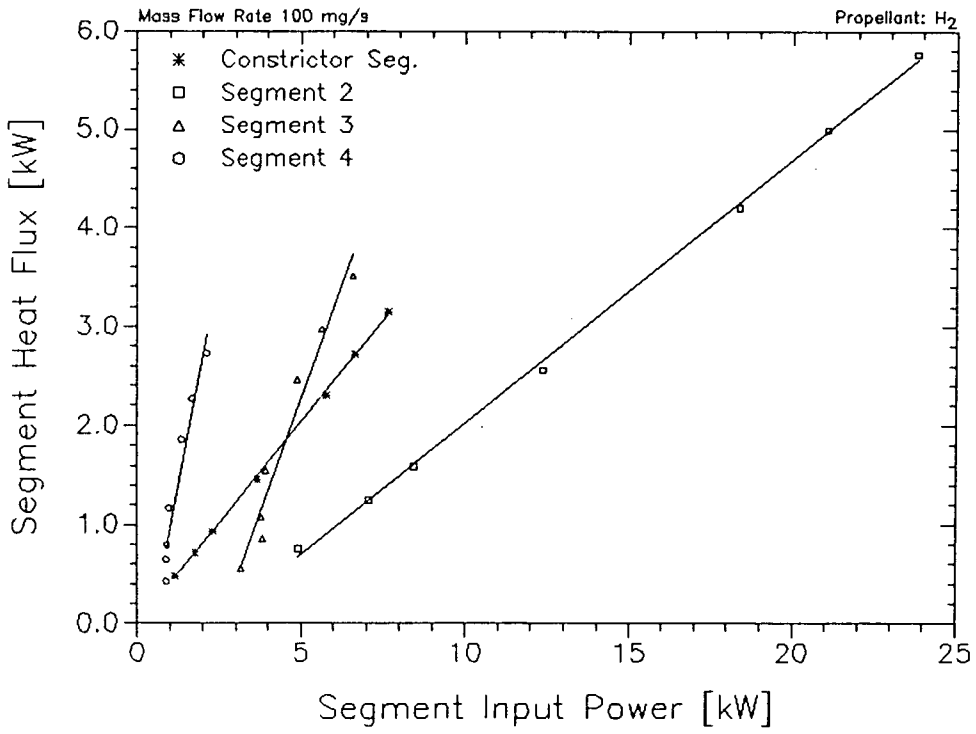

Figure 21: Segment heat flux versus input power at 100 mg/s

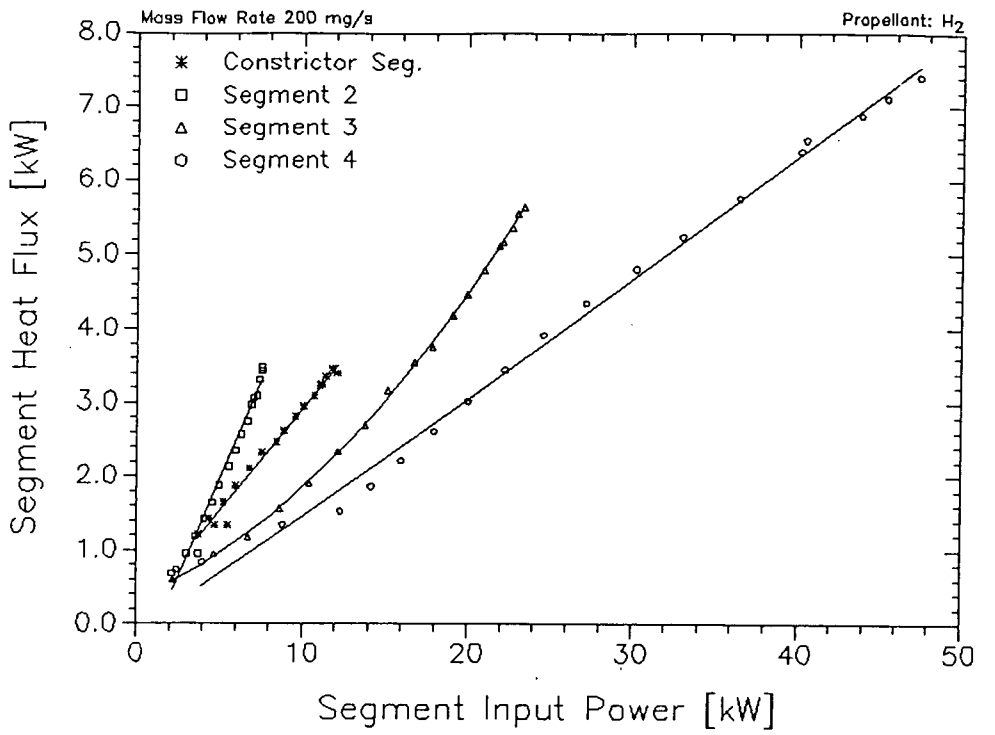

Figure 22: Segment heat flux versus input power at 200 mg/s

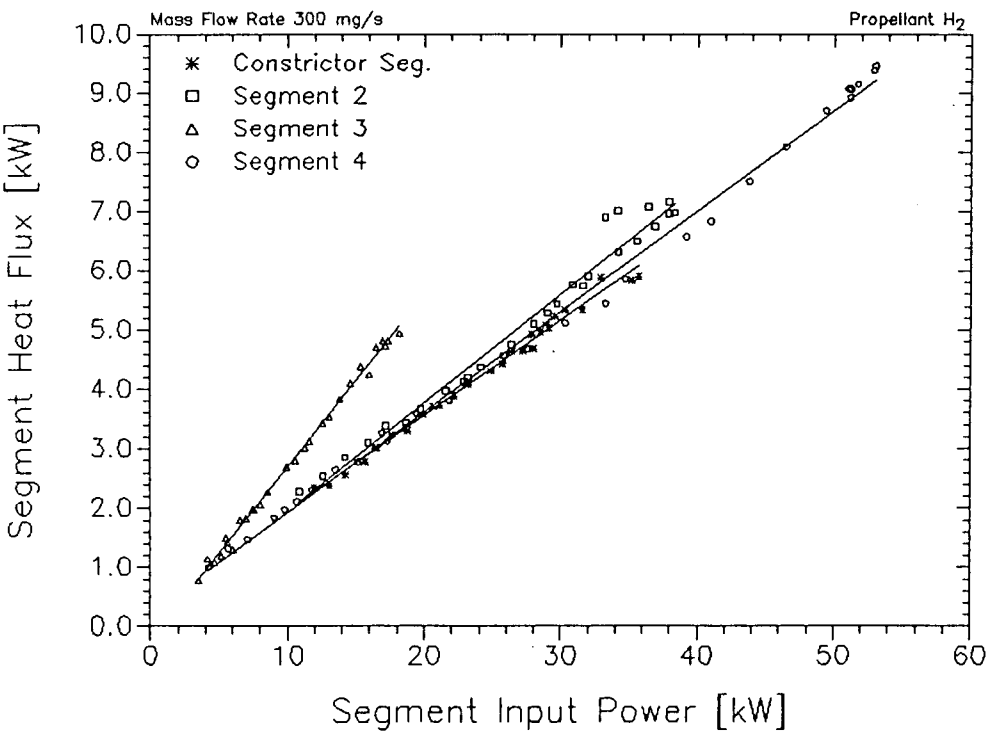

Figure 23: Segment heat flux versus input power at 300 mg/s

References

[1] HIPARC, High Power Arcjet, M. Auweter-Kurtz et al., Institut für Raumfahrtsysteme, University of Stuttgart, IRS 89-P19, First Progress Report, NASA Grant No. NAGW–1736, October 1989

[2] Medium Power Arcjet Thruster Experiments, B. Glocker et al., Institut für Raumfahrtsysteme, University of Stuttgart, AIAA 90-2531, July 1990

[3] High Power Arcjet, M. Auweter-Kurtz et al., Institut für Raumfahrtsysteme, University of Stuttgart, IRS 90-P7, Second Progress Report, NASA Grant No. NAGW–1736, August 1990